EXPERIMENTAL STUDY OF SHEAR AND COMPACTION BAND FORMATION IN BEREA SANDSTONE

A Thesis

by

ELIZABETH ANNE HERRIN

Submitted to the Office of Graduate Studies of
Texas A&M University
in partial fulfillment of the requirements for the degree of

MASTER OF SCIENCE

December 2008

Major Subject: Geology

EXPERIMENTAL STUDY OF SHEAR AND COMPACTION BAND FORMATION IN BEREA SANDSTONE

A Thesis

by

ELIZABETH ANNE HERRIN

Submitted to the Office of Graduate Studies of
Texas A&M University
in partial fulfillment of the requirements for the degree of

MASTER OF SCIENCE

Approved by:

Chair of Committee,	Frederick M. Chester
Committee Members,	Judith S. Chester
	David Schechter
Head of Department,	Andreas Kronenberg

December 2008

Major Subject: Geology

ABSTRACT

Experimental Study of Shear and Compaction Band Formation in Berea Sandstone.

(December 2008)

Elizabeth Anne Herrin, B.S., Texas A&M University

Chair of Advisory Committee: Dr. Frederick M. Chester

Many field, experimental, and theoretical studies have contributed greatly to our understanding of the occurrence and formation of deformation bands in porous granular materials, but questions remain regarding the mechanics of strain localization, and how the orientation, thickness and internal strain (shear relative to volume change) of deformation bands is influenced by loading history and evolving rock properties. Here we report on triaxial rock deformation experiments using a non-traditional sample geometry to investigate band formation across the brittle-ductile transition. Five-cm diameter cylinders of Berea sandstone were machined with a circular (8.77 cm radius) notch to form a dog-bone sample geometry. In triaxial compression, the sample geometry obviates end-effects without creating heterogeneous stress gradients that can influence localization. Samples were instrumented to measure local strains in the neck region and acoustic emissions (AE), and then shortened to failure at confining pressures of 50 to 250 MPa. Deformation bands formed at all conditions, and photo mosaics of the outer sample surface were used to determine the thickness and orientation of the bands. Band thickness increases from several to tens of mm thickness and the angle

between the bands with the shortening axis changes from 35 to 80 degrees, as confining pressure increases from 50 to 250 MPa, respectively. Mechanical data, including local strain measurements through yield, were used to test theoretical models for the onset of localization and formation of deformation bands as an instability in the constitutive description of homogeneous deformation. Generally, theoretical predictions compare favorably with the observed onset of localization determined by marked changes in the AE rate, and are consistent with the formation of compacting shear bands at higher mean stress. Predictions of changes in band orientation with mean stress are largely consistent with observed trends, but deviate from the observed orientation by as much as twenty degrees.

TABLE OF CONTENTS

Page

ABSTRACT iii

TABLE OF CONTENTS v

LIST OF FIGURES vii

LIST OF TABLES ix

1. INTRODUCTION 1

2. PREVIOUS WORK 5

    2.1 Field Observations 5
    2.2 Experimental Studies 6
    2.3 Theoretical Models 8

3. METHODS 11

    3.1 Rock Type Description 11
    3.2 Sample Geometry 11
    3.3 Sample Preparation and Jacketing 12
    3.4 Experimental Apparatus and Procedure 14
    3.5 Observation of Deformed Samples 15

4. RESULTS 16

    4.1 Mechanical Data 16
    4.2 Deformation Band Characteristics 22

5. DISCUSSION 29

    5.1 Experimental Determination for the Onset of Localization 29
    5.2 Macroscopic Failure Envelope 31
    5.3 Predicting the Onset of Localization 35
    5.4 Predicting Fracture Orientation 43

6. CONCLUSION 46

Page

REFERENCES 48

VITA 51

LIST OF FIGURES

FIGURE		Page
1	Macroscopic failure envelope for a porous sandstone in deviatoric versus mean stress space	3
2	The sample assembly	13
3	Failure curves for Berea sandstone	18
4	The AE-rate versus axial strain curve	20
5	Comparison of stress-strain curves for local axial (red curve), radial (blue curve), and volumetric strains (green curve)	21
6	Photograph of sample deformed at a confining pressure of 50 MPa	25
7	Photograph of sample deformed at a confining pressure of 100 MPa	26
8	Photograph of sample deformed at a confining pressure of 150 MPa	27
9	Thickness of deformation bands plotted against mean stress	28
10	Comparison of differential stress and AE-rate during differential loading for confining pressure of 200 MPa (local axial strain)	30
11	Macroscopic yield envelope fit to triaxial experimental data for Berea sandstone	34
12	Comparison of AE-rate, differential stress, axial strain rate, and hardening modulus during triaxial compression loading of Berea sandstone at confining pressure of 50 MPa	38
13	Comparison of AE-rate, differential stress, axial strain rate, and hardening modulus during triaxial compression loading of Berea sandstone at confining pressure of 150 MPa	39

FIGURE Page

14 Comparison of AE-rate, differential stress, axial strain rate, and hardening modulus during triaxial compression loading of Berea sandstone at confining pressure of 200 MPa 40

15 Recreation of the failure mode map for shear bands..... 42

LIST OF TABLES

TABLE		Page
1	Experimental results	17
2	Stress and strain at macroscopic yield	33
3	Dilatancy factor and slope of failure envelope	36
4.	Comparing the observed band orientation to the predicted band orientation	45

1. INTRODUCTION

Deformation bands are zones of localized shear displacement with variable amounts of compaction and dilation; however, they can be, in theory, completely compactant or dilatant with no amount of shear displacement [1, 2, 3]. Compaction shear bands within a high porosity sandstone are characterized as zones of grain crushing, densification, and a reduction in porosity [1, 2, 4]. Compaction bands act as low permeability barriers restricting fluid flow in reservoir sandstones, an effect that is important to the exploration for water and hydrocarbons [1, 3, 5].

The experimental characterization of failure and localization of a porous material is often depicted in stress space where the yield stresses are mapped out to define a yield envelope. The failure mode is dependent of the dilatant or compactant inelastic behavior of the rock at different mean stresses [6]. Samples deformed at low to medium mean stresses fail by shear enhanced dilation, while those deformed at high mean stresses fail by shear enhanced compaction [1, 5]. The stresses for dilatant localization plot along a yield envelope with an approximate constant positive slope – this is Coulomb behavior. Compactant localized deformation is associated with a yield cap [1, 7, 6] that has a negative slope [1, 8]. Two load paths, one at medium mean stresses and one at high mean stresses, are depicted on Figure 1 to show the condition for the two failure modes.

This thesis follows the style of *International Journal of Rock Mechanics and Mining Sciences.*

Deformation experiment results suggest there is a continuous transition between shear enhanced dilation to shear enhanced compaction as the mean stresses increase that is referred to as transition from brittle to ductile deformation (BDT) [6, 9]. Macroscopic failure observed for a sample deformed in the BDT has both conjugate shear fractures and barreling of the sample [10].

Rudnicki and Rice's [11] model localization as an instability in homogenous deformation. This model predicts that localization will occur at a critical hardening of the sample and in a specific orientation which depends on several parameters, including the deviation of local strains from purely elastic deformation, the dilatancy parameter (β), and the slope of the yield envelope (μ') that reflects the pressure sensitivity of inelastic yielding [10, 11]. The original bifurcation analysis failed to consider localization within a porous media, and therefore did not explore the concept of shear enhanced compaction bands. Olsson [1] determined that the bifurcation analysis could be applied to study compaction bands in porous sandstones. He found that compaction bands form at high mean stresses with a negative yield-envelope slope (consistent with the cap model) and a low magnitude positive to negative dilatancy factor.

Many suites of experiments have been conducted in order to study the formation and evolution of deformation bands at different stresses past failure and the parameters important to understanding band development. In order to better understand the evolution of deformation bands within experimental samples, AE can be recorded to monitor relative deformation [5, 12] and x-ray computed tomography can be used to characterize density differences within the sample [9]. In many of the previous

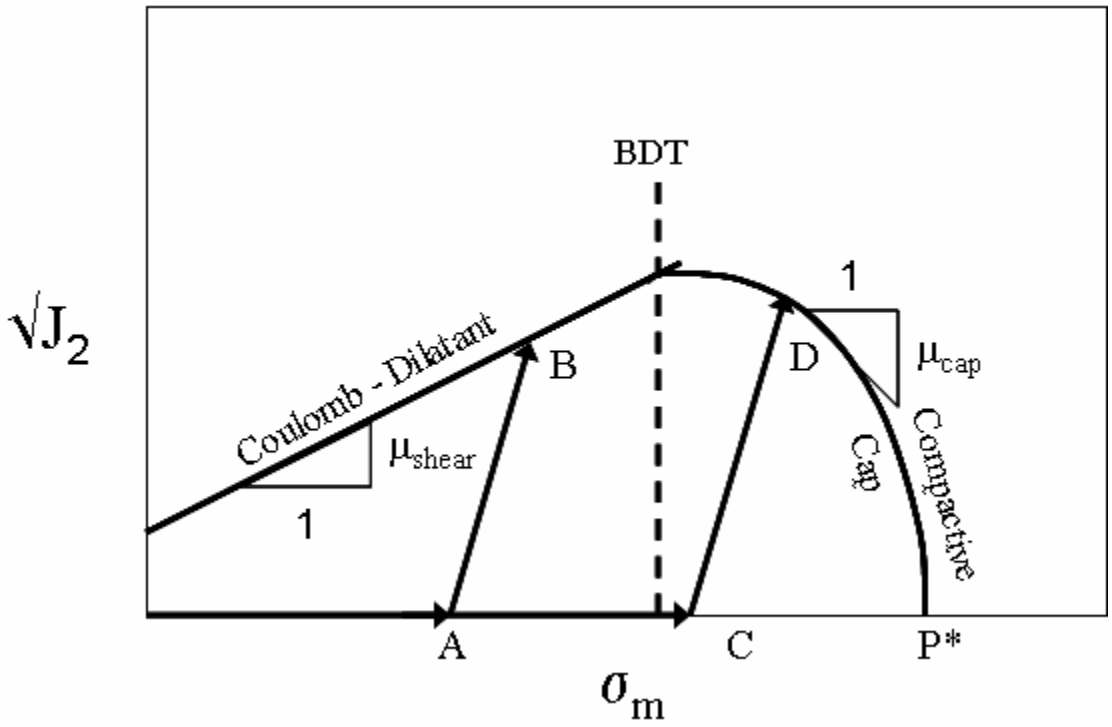

Figure 1. Macroscopic yield envelope for a porous sandstone in deviatoric versus mean stress space. Coulomb dilatant failure is marked by the straight line at low mean stress and the onset of compactive yield is marked by an elliptical yield cap at high mean stress. The transition from dilatant shear bands to compactant shear bands is thought to occur in the brittle ductile transition zone [5]. The load paths AB and CD represent triaxial load paths, points B and D represent the condition for macroscopic failure and the onset of localization. When loading continues past D, the sample will begin to develop shear bands. Redrafted from Olsson [1].

experiments, much of the deformation has occurred in the ends of the samples where stresses are very heterogeneous and stress states are poorly understood (as seen in Olsson [1] and Besuelle [9]). Vadjova and Wong [13] employed a sample type that forced the deformation band to propagate in the neck of the sample away from the ends by creating a v-notch in the sample. This geometry creates a marked stress heterogeneity in the neck of the sample and permits study of band propagation, but it does not allow study of the instability in homogeneous deformation as described by Rudnicki and Rice's [11] bifurcation analysis because of the strongly heterogeneous stress. This geometry also prevents local strains from being measured, which is necessary to test the theoretical models.

The suites of experiments presented in this research utilize a geometry previously used for extensional experiments (dogbone geometry) in order to test theories for the formation of deformation bands in compression. The dogbone geometry removes the problem of end effects, but still allows for fairly homogeneous deformation in the neck region with smoothly varying stress and strain conditions. The purpose of this study is to test mathematical predictions for the onset of localization and the orientation of deformation bands.

2. PREVIOUS WORK

The formation of deformation bands was first modeled by Rudnicki and Rice [11] as an instability in the constitutive description of homogeneous deformation. This model defined the relevant mechanical conditions necessary for localized failure modes to develop. These conditions include the isotropic hardening of a material where inelastic dilatancy and hydrostatic stress strongly influence the yield criterion in brittle rocks, the dilatancy factor (β), and the slope of the yield surface (μ'). The initial model for the formation of deformation bands did not consider the mechanical behavior for porous materials and excluded the formation of a compactant end member.

2.1 Field Observations

Deformation bands have often been described in high porosity sandstones as tabular zones of low porosity that display positive relief in outcrops [2, 3, 4, 14, 15]. The presence of the deformation bands in a sandstone is associated with some amount of shear displacement with variable amounts of dilatancy or compaction. Microstructural characterization of these deformation bands show that there is much grain crushing and pore collapse [4, 14]. Mollema and Antonellini [2] were the first to identify "pure" compaction bands in the field that showed no shear displacement and were oriented sub-perpendicular to the maximum principal stress. Compaction bands are of great interest because they can act as fluid flow barriers [3], controlling the manner in which fluids can pass through a reservoir sandstone and creating compartmentalized reservoirs [1].

There is also evidence that compaction bands created in one stress regime can be "overprinted" by styolites [16] or joint sets as local stress conditions change [3, 15]

2.2 Experimental Studies

Olsson [1] was one of the first to consider Mollema and Antonellini's [2] description of compaction bands in the field and realize that the original bifurcation analysis could include porous sandstones. Rudnicki and Rice [11] considered only a positive dilatancy factor for the formation of deformation bands. Olsson [1] stated that for compaction bands to form, $\beta + \mu = -\sqrt{3}$, such that the dilatancy factor has a low-positive to negative magnitude. When the associated yield cap at high mean stresses is considered, a low-positive to negative μ' is possible. Olsson [1] conducted a suite of experiments at confining pressures, P_c, of 69 MPa to 100 MPa to determine these parameters and the strains necessary to initiate compaction bands. In order to successfully predict the orientation of the compaction band, Olsson [1] was forced to estimate values for β and μ' rather than measure the values directly. If β and μ' could be accurately determined from experimental results, the theoretical prediction of the orientation of compaction bands may better coincide with observed orientations.

Besuelle et al. [17] used axial and radial strain gages to measure the volumetric changes that occur in the deformed sample and to determine the moment that the homogeneity of the strain field associated with the onset of localization is lost. In addition, changes in porosity in the specimens may be characterized post-experiment using X-ray CT to show that there is an increase in porosity around the bands at low confining pressures, and a decrease in porosity around the shear bands at higher

confining pressures. This increase and decrease in porosity relate to dilatant and compactant deformation bands, respectively. Later theoretical analyses of strain localization done by Besuelle [9] show that there is a continuous variation of the strain conditions between shear bands and pure dilation or compaction bands.

Acoustic emission activity has been used to analyze the processes of localization in a sandstone [5, 12, 18, 19]. DiGiovanni [12] showed that there are two peaks in AE activity relating to two stages of compaction within the samples: The first stage was due to grain boundary breakage and rotation related to poor cementation in the sample; the second was a result of continued rotation and intense grain cracking. According to the AE data, the initial deformation propagated at the specimen ends. The second stage of compaction propagates as a localized deformation band as the sample deforms at near constant deviatoric stress.

It has been noted that the propagation of compaction bands within a triaxially compressed sample often occurs in the ends of the specimen due to the stress concentrations caused by the pistons (as seen in Olsson [1], Wong et al. [5], DiGiovanni [12], and Besuelle et al. [17]). This greatly complicates comparison of laboratory experiments with theory because the local stress at the sample ends is not well understood. V-notched samples have been used to analyze the effect of a local stress concentrator on the propagation of compaction bands [13, 19]. Understanding the effect of this stress concentrator has many implications for the effect of local heterogeneities and how they affect the initiation of compaction within a rock mass. Compaction localization originates at the notch tips and propagates through the sample at a lower

mean stress than that required for a cylindrical sample [19]. Analyses of data for two different types of sandstones suggests that the processes that control the propagation of compaction bands relate to differences in mineralogy, compaction, cementation, and other rock properties [12, 19]. Although this geometry forces propagation away from the sample ends, the localized stress states and strain conditions can not be directly measured.

2.3 Theoretical Models

Wong et al. [5] characterized the microstructural damage associated with compaction bands and conjugate shear bands in porous rock samples with a focus on the brittle-ductile transition zone. They concluded that damage due to localized failure within the transitional regime occurs by two mechanisms: axial microcracks that may later form shear cracks, and grain crushing that leads to a reduction in porosity. The deformation observed was determined to be a hybrid of shear bands and compaction. Based on these findings, Wong et al. [5] argued that the original bifurcation analysis done by Rudnicki and Rice [11] should be reanalyzed to consider the change in the macroscopic damage mechanisms from the brittle to ductile regimes as well as volumetric changes caused by mean stress.

A yield cap is thought to exist in τ-σ space which defines the condition where inelastic volume strain is yielding, as depicted in Figure 1 [1, 6, 7]. Rudnicki [8] modeled the conditions of compaction localization for stress states on an elliptical yield cap. This yield cap is characterized by a decrease in shear stress with an increase in compressive mean stress [1]. Rudnicki [8] considered negative values for β and μ' along

with two other parameters: the slope of the hydrostatic stress versus strain curve associated with the onset of localization (k_{crit}) and the lateral confining pressure, σ_c. When comparing the predicted confining stress for the transition and the observations from experimental studies done by Wong et al.[6], Baud et al. [18], and others. Rudnicki [8] noted that the transition stresses determined in the lab were often less than the theoretical values and attributed the discrepancies to several factors. One problem is that the model calculates the transition values based on an initial yield surface, which does not account for changes in the yield condition as the inelastic strain in the sample changes. Also, the form of the elliptical surface does not describe the distinct microscopic processes of deformation or the effects of microstructural elements that may affect the onset of localization (e.g. DiGiovanni et al. [12]; Baud et al. [18]). In addition, Rudnicki [8] stated that the compaction bands observed at confining pressures below the transition values are likely a combination of distributed compaction as well as low angle shear bands.

Rudnicki's [8] analysis raises many questions. Can compaction bands be differentiated from the low-angle shear bands formed in the B-D transition? The predicted values of P_c (or σ_m) for the transition in Berea sandstone range from 268-313 MPa; however, the highest confining pressure tested by Baud et al. [18] was only 200 MPa, where discreet and diffuse compaction bands were observed. What is the character of localization that occurs at the predicted transition confining stress? If an experimental geometry is employed that causes deformation to occur away from the sample ends, but

also allows local strains to be measured, will the experimental observations compare favorably with theoretical models?

3. METHODS

3.1 Rock Type Description

Berea sandstone, from Cleveland Rock Quarries in Ohio [20], was chosen for this study because the mechanical behavior is well studied and shows good reproducibility. Samples used in this study are similar to those used by Bobich [20], and have a porosity of 19% and a mean grain diameter of 185 μm. The sandstone has well sorted, subangular grains composed of 75-80% quartz, 20-25% feldspar, dolomite, rutile, zircon, and kaolinite, and other secondary minerals [20]. Dark laminae made up of mafic minerals are present in the sandstone.

3.2 Sample Geometry

Previous experiments exploring the conditions of deformation band formation used a cylindrical sample geometry [1, 5, 12, 17]. Much of the deformation in the samples from these experiments occurred in the sample ends where the stress fields are poorly understood. In order to force deformation to occur away from the sample ends, a dog-bone, or notch-cut, sample geometry is used for the experiments reported herein. Initially used in extension experiments, the notch-cut geometry has been used by Ramsey and Chester [21] and Bobich [20] for the study of fracture under mixed tensile and compressive stress states. Samples have a cylindrical form with a neck diameter that is smaller than the shoulder diameter. The smaller neck diameter will cause deformation bands to initiate and propagate in the neck rather than at the sample ends without introducing heterogeneous stresses to the sample.

3.3 Sample Preparation and Jacketing

Dog-bone samples were created by taking approximately 12.7 cm long, 5 cm diameter cores from blocks of Berea sandstone. Samples were cored parallel to the laminations present in the rock to facilitate the preparation of the notch-cut and to minimize the affects of lamination on band orientation. Samples were clamped in a microlathe positioned on the movable bed of a stationary-wheel surface grinder. The cores were ground in two stages. Initial machining is done on samples rotating on an axis parallel the axis of rotation of the grinding wheel in order to remove large amounts of material to form the notch. Samples were then rotated 90º and ground to create a smooth notched surface on the samples. The final samples are approximately 10.16 cm long, with a sample shoulder diameter of 4.686 cm (±0.007 cm), a neck diameter of 3.033 cm (±0.0076 cm).

In normal triaxial deformation experiments, a polyolefin jacket is used to prevent the confining fluid from permeating the sample. According to Bobich [20], the polyolefin jacket creates a load on the sample influencing strength data and failure mode. To prevent this effect, a multilayered jacket as described by Bobich [20] and Ramsey and Chester [21] was employed (Figure 2). In the multilayer, the outermost polyolefin jacket is used to prevent the confining media from coming in contact with and saturating the sample. To keep the polyolefin jacket away from the sample, plasticene modeling clay is packed around the sample neck flush to the shoulders. An innermost jacket of latex is used to prevent the clay from intruding into the pore space of the

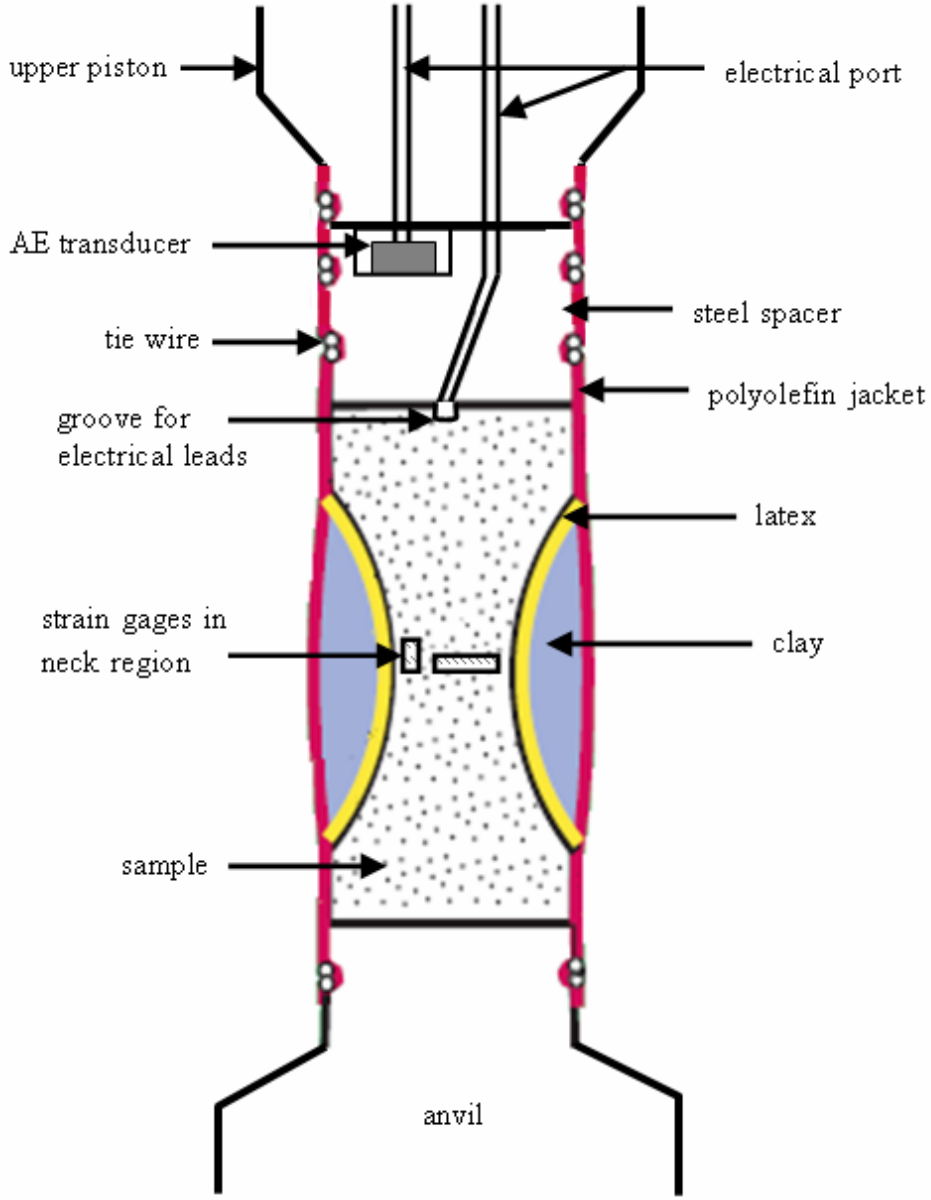

Figure 2. The sample assembly. A three layer jacketing system is used for the samples: A polyolefin jacket is used to prevent the confining fluid from saturating the sample. Because the polyolefin affects the strength data, clay surrounds the sample to separate it from the polyolefin. Latex is used as the inner jacket to prevent the clay from intruding into the sample. This jacketing configuration is modeled after Bobich [20]. The sample is affixed to the anvil at the bottom, and the upper piston at the top using tie wires. There is a steel spacer attached to the upper piston that contains the AE transducer (or the transducer is placed at the other end of the upper piston). The electrical port on the left contains the leads from the transducer, the one on the right holds the leads from the strain gages. Assembly not drawn to scale.

sandstone. Nichrome wire is used to secure the polyolefin jacket to the upper piston and lower anvil.

3.4 Experimental Apparatus and Procedure

Samples are deformed in the Large Specimen Rig (LSR) of the John Handin Deformation Lab. The LSR is a liquid confining media, gear driven, triaxial apparatus with a digital data acquisition system that records axial force, axial displacement, confining pressure, and acoustic emissions (AE). A jacketed sample secured to the upper piston and lower anvil is placed in the pressure vessel and compressed at a confining pressure of 50-300 MPa and at an axial displacement rate of 2.5 μm/s. At this rate, experiments typically run for 15-20 minutes in duration from the hit point to macroscopic failure and data is collected at a rate of 1.3 Hz. During the experiment, the confining pressure may decrease as much as 10-30 MPa due to changes in volume of the sample. Samples are shortened past yield as determined by the stress-strain behavior.

Initially, AE data was recorded using a Lead Zirconate Titanate piezoelectric transducer affixed to the spacer adjacent to the sample; however, for the majority of tests the AE transducer was affixed to the force gage at the other end of the upper piston, approximately 25 cm from the original placement. The increase in distance from the sample is reflected by a reduction in the recorded rate of AE up to 100-200 counts per second. Regardless of the AE transducer placement, the changes in relative AE-rates over the course of an experiment are very similar for experiments run at the same confining pressure.

In several experiments, strain gages are used to measure the axial and radial strains in the neck of the sample. Four 350 Ω gages (two to measure axial and two to measure radial strains) are affixed to the surface of the samples using epoxy that is cured for a minimum of six hours at room temperature. Strain-gage electrical leads were fed through ports in the piston along grooves cut in the sample so they would not interfere with the piston. Grooves were filled with epoxy and copper foil was placed between the polyolefin jacket and the grooves to prevent jacket leaks. Signals from wheatstone bridges incorporating the strain gages were amplified, filtered, and recorded throughout the experiments using a strip chart, and changes in strain during the experiment are accurate to 0.5% of the total voltage.

3.5 Observation of Deformed Samples

After deformation, samples were removed from the LSR and the jackets carefully cut away. Serial photographs of the outer cylindrical surface of the samples were taken at 15º intervals and merged to create a 360º view of the deformation bands (Figure 6). Orientation of the shear bands was determined by fitting sinusoids to the features seen in the photographs.

4. RESULTS

A total of ten successful experiments were completed: nine of which have recorded AE data, three with local strain data from strain gages recorded, and four were photographed (Table 1).

4.1 Mechanical Data

The stress-strain curves show an increase in differential stress with confining pressure and good reproducibility between experiments (Figure 3a). The curves display non-linear elastic behavior followed by yielding and then either a stress drop or strain hardening reflecting brittle behavior or ductile behavior, respectively. Dogbone samples of Berea sandstone in compression exhibit brittle behavior at confining pressures of 50 MPa, transitional behavior at confining pressures from 100-150 MPa, and ductile behavior above 200 MPa.

Figure 3b compares stress-strain curves at 50 MPa and 200 MPa for axial strain determined over the total length of the samples and for axial strain measured by strain gages in the neck region of the sample. As expected, the curves show greater axial strain in the neck of the sample than that averaged over the length of the sample at the same differential stress. The samples deformed at 50 MPa show good reproducibility of yield strength, whereas those deformed at 200 MPa show significant variability in yield strength (7% difference) and in ultimate strength (11% difference).

The onset of AE activity correlates with deviation from purely elastic behavior at 50-70% of macroscopic failure strength. As a sample is progressively loaded, there is an

Table 1
Experimental results

Exp #	Initial Confining Pressure (MPa)	Final Axial Strain (%) *	AE Data	Strain Gage Data	Sample Photographed
4911	50	1.24	U	No	Yes
4918	50	1.34	U	Yes	No
4910	100	1.46	U	No	Yes
4906	150	1.8	S	No	Yes
4919	150	2.04	U	Yes	No
4908	200	2.44	S	No	No
4909	200	4.78	None	No	No
4920	200	1.77	U	Yes	No
4912	250	2.19	U	No	Yes

U = data measured from opposite end of upper piston

S = data measured from steel spacer

* axial strain calculated for the total length of the sample

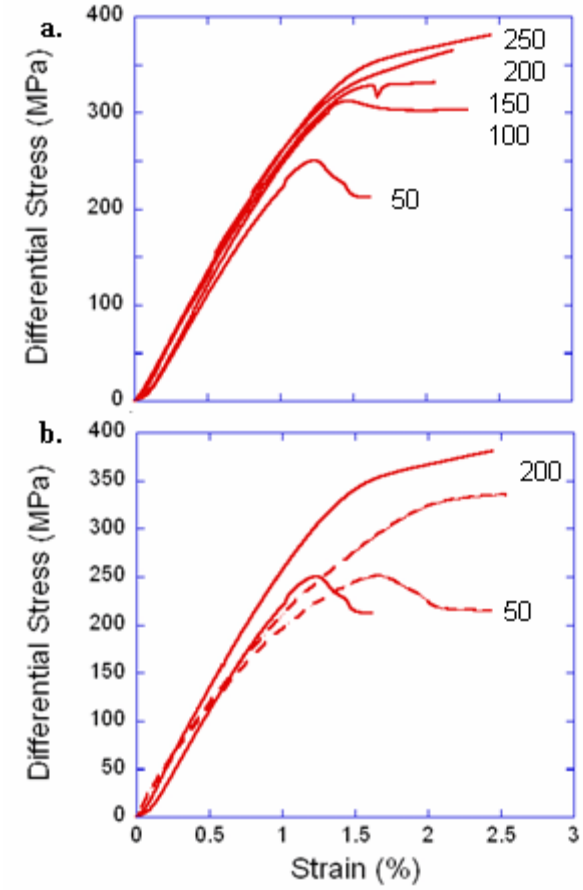

Figure 3. Failure curves for Berea sandstone. The solid failure are for axial strains averaged over the length of the sample. Dashed failure curves represent axial strains measured locally in the neck of the sample.

increase in AE-rate up to the load approximately correlating with macroscopic failure, i.e. ultimate strength in the brittle field or sharp deviation from elastic loading in the ductile field. For samples deformed at low confining pressures (i.e. 50 MPa), the AE-rate versus axial strain curve shows an obvious and abrupt change from positive to negative slope approximately corresponding to macroscopic failure. The slope of the AE-rate curve post yield is less negative with increase in confining pressure. The AE-rate associated with deformation at high confining pressures approaches a constant rate after macroscopic failure (Figure 4). AE-rates are expressed as counts per second, peak rates range up to 200 to 300 counts per second using the second AE system configuration, and there is no correlation between confining pressure and cumulative counts.

The strain gages placed to measure changes in circumference in the neck of the sample during differential loading recorded circumferential lengthening and radial expansion, i.e., negative radial strain (Figure 5). Radial strains at yield range from -0.35 to -0.70% as confining pressure increases from 50 to 200 MPa. During initial compression of each sample, there is very little change in the radial strain. As the sample approaches failure, there is a marked change in radial strain indicating that the neck of the sample is expanding inelastically by microcracking as recorded by the corresponding increase in AE-rate. The strain gages placed to measure changes in the length of the neck of the sample during differential loading recorded axial shortening of the neck of the sample, i.e., positive axial strain. Local axial strains at yield range from 1.48 to 2.29% as confining pressure increases from 50 to 200 MPa. The volumetric

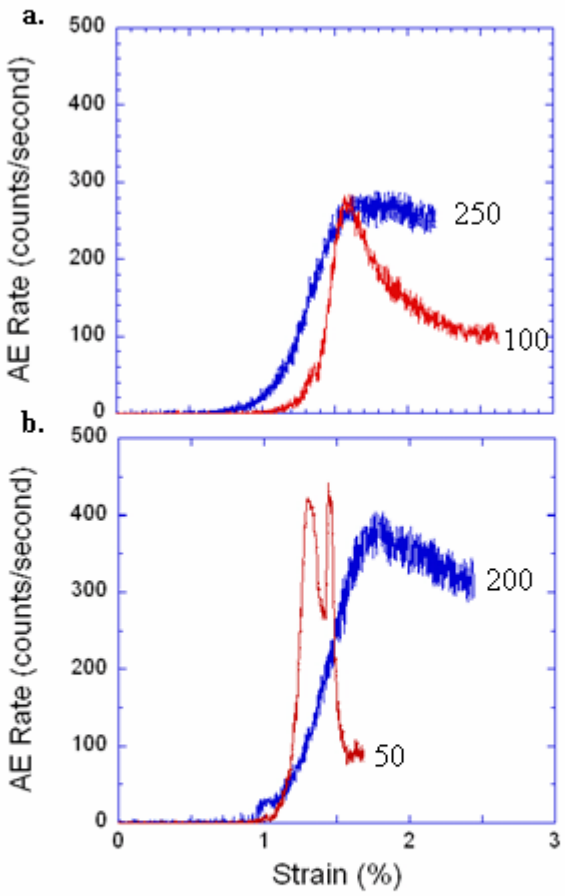

Figure 4. The AE-rate versus axial strain curve. The shape of the curve changes depending on the confining pressures. At lower confining pressures, the curve has a peak and then sharp negative slope. For experiments at higher confining pressures, the curve approaches a constant rate. Strains are averaged over the length of the sample.

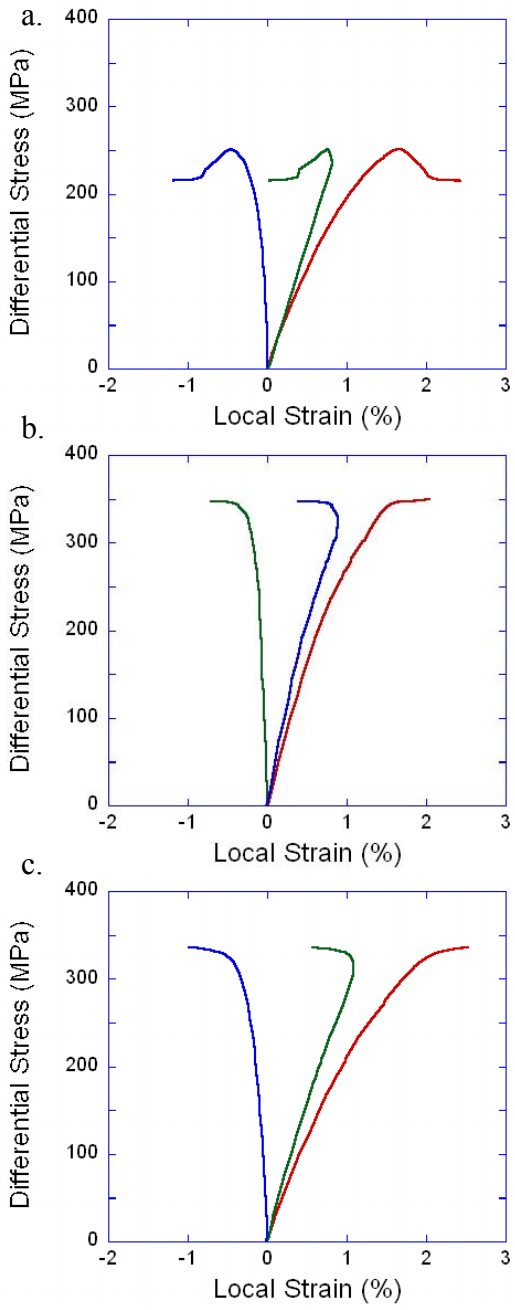

Figure 5. Comparison of stress-strain curves for local axial (red curve), radial (blue curve), and volumetric strains (green curve). (a) Confining pressure is 50 MPa. (b) Confining pressure is 150 MPa. (c) Confining pressure is 200 MPa.

strain is calculated from the axial and radial strains such that

$$\varepsilon_{vol} = \varepsilon_{ax} + 2\varepsilon_{rad}$$

[10]. The volumetric strain versus differential stress curve shows that, for all three experiments, the sample is contracting as the differential stress increases until the deformation becomes dilatant just before macroscopic failure is achieved.

Using the local strain, the Young's modulus is determined by finding the tangent modulus measured over a portion of the differential stress versus axial strain curve between 20-40% of the ultimate strength. At a confining pressure of 50 MPa, the tangent modulus is 22 GPa; at 150 MPa, it is 28.0 GPa; and at a confining pressure of 200 MPa, it is 20.8 GPa.

4.2 Deformation Band Characteristics

The orientation of a deformation band is described as the angle from the maximum compression to the band. For a pure-compaction band, deformation band orientation should be at or near 90º. Although samples were cored parallel to the sandstone laminations to minimize the effect of lamination on deformation band formation, the laminations do influence the band orientation. The intersection of the bands with the maximum-compression principal-plane is generally parallel to the laminations, i.e. bands strike parallel to the laminations (Figure 6). Band angles increase from 35º to 78º as confining pressures increase from 50 to 250 MPa.

The bands described here represent samples that were deformed past macroscopic failure at similar axial strains. For samples deformed at 50 MPa, two distinct, intersecting deformation bands less than 2 mm thick are present (Figure 6). The

sample deformed at 100 MPa is characterized by a single, thicker band of deformation where the intersection of the band with the sample surface displays a sugary texture (Figure 7). The deformation band associated with confining pressure of 150 MPa is slightly thicker than that at 100 MPa and also consists of a single band that is characterized by a sugary texture on the surface of the sample (Figure 8). The deformation band formed at 200 MPa is approximately the same width as that formed at 150 MPa with a similar sugary texture. The sample deformed at 250 MPa displays a single, thick deformation band that is only distinguishable from the rest of the sample by a lighter color and slightly sugary texture on the surface of the sample. All of the samples have a fracture present within and coplanar to the deformation band, the fracture likely forms during unloading and removal of the sample from the pressure vessel, and forms within the band because it is a zone of reduced cohesion.

Baud et al. [18] noted that compaction bands that form in Berea sandstone can form as discreet or diffuse bands as the confining pressure increases. Discreet bands are defined as narrow bands approximately the width of grain diameter and diffuse bands are broad zones of deformation that can scale 6-8 times grain diameter [18]. This is qualitatively similar to the character of bands observed in samples deformed for this study. The width of the deformation band increases with increasing confining pressure up to approximately 22 mm (Figure 9). At confining pressure of 50 MPa, the deformation bands are narrow bands, about 2 mm thick, approximately 10 times the diameter of the grains. As the pressure is increased to 100 MPa, the bands become more

diffuse with a width of approximately 15 mm. For confining pressures from 150-250 MPa, the width of the band is approximately 20-22 mm.

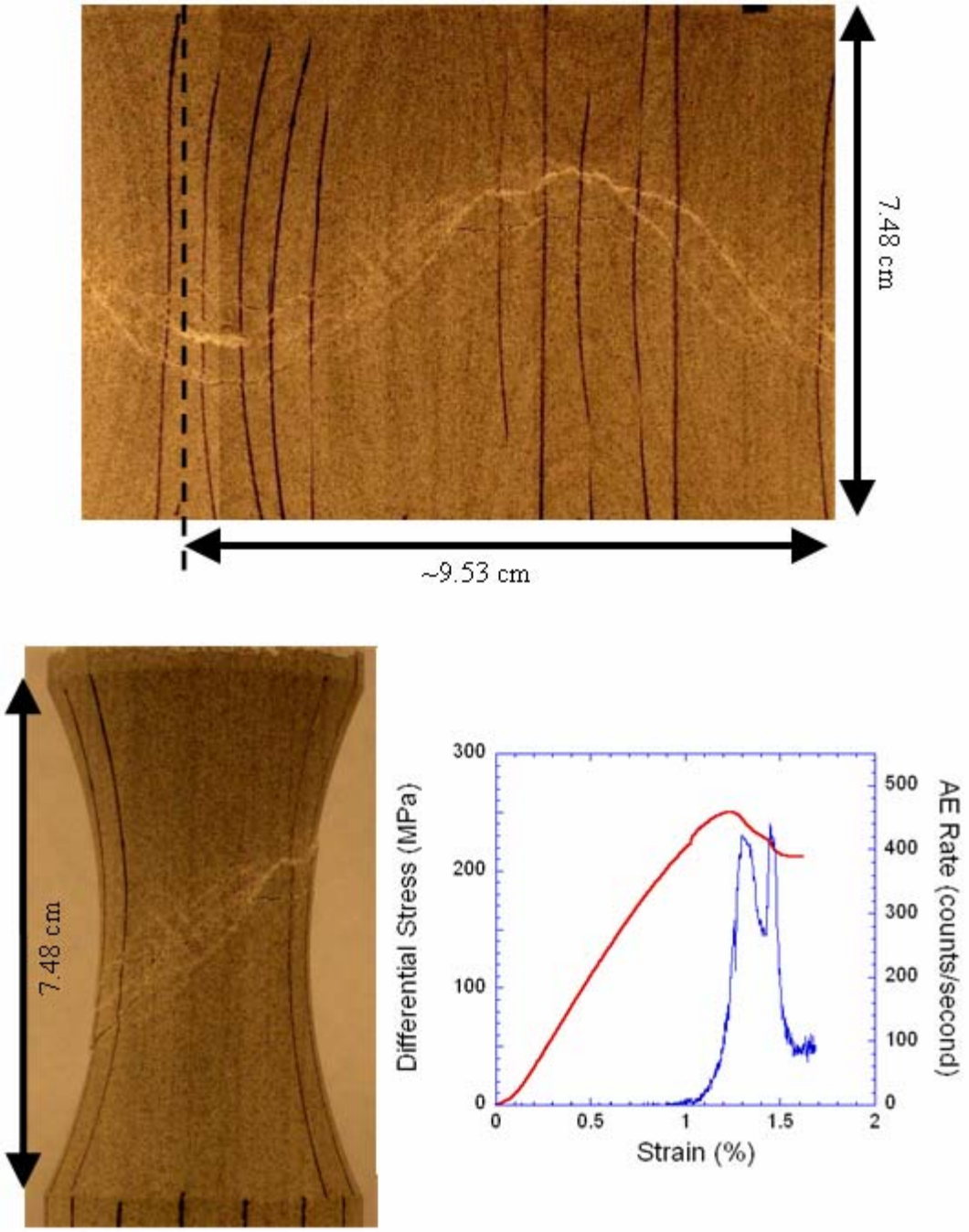

Figure 6. Photograph of sample deformed at a confining pressure of 50 MPa. The upper photograph is a composite of photos taken every 15º. The zone of deformation is marked by two distinct shear bands. The dashed line in the upper photograph indicates where the photo begins to repeat. 1:1 ratio height to width.

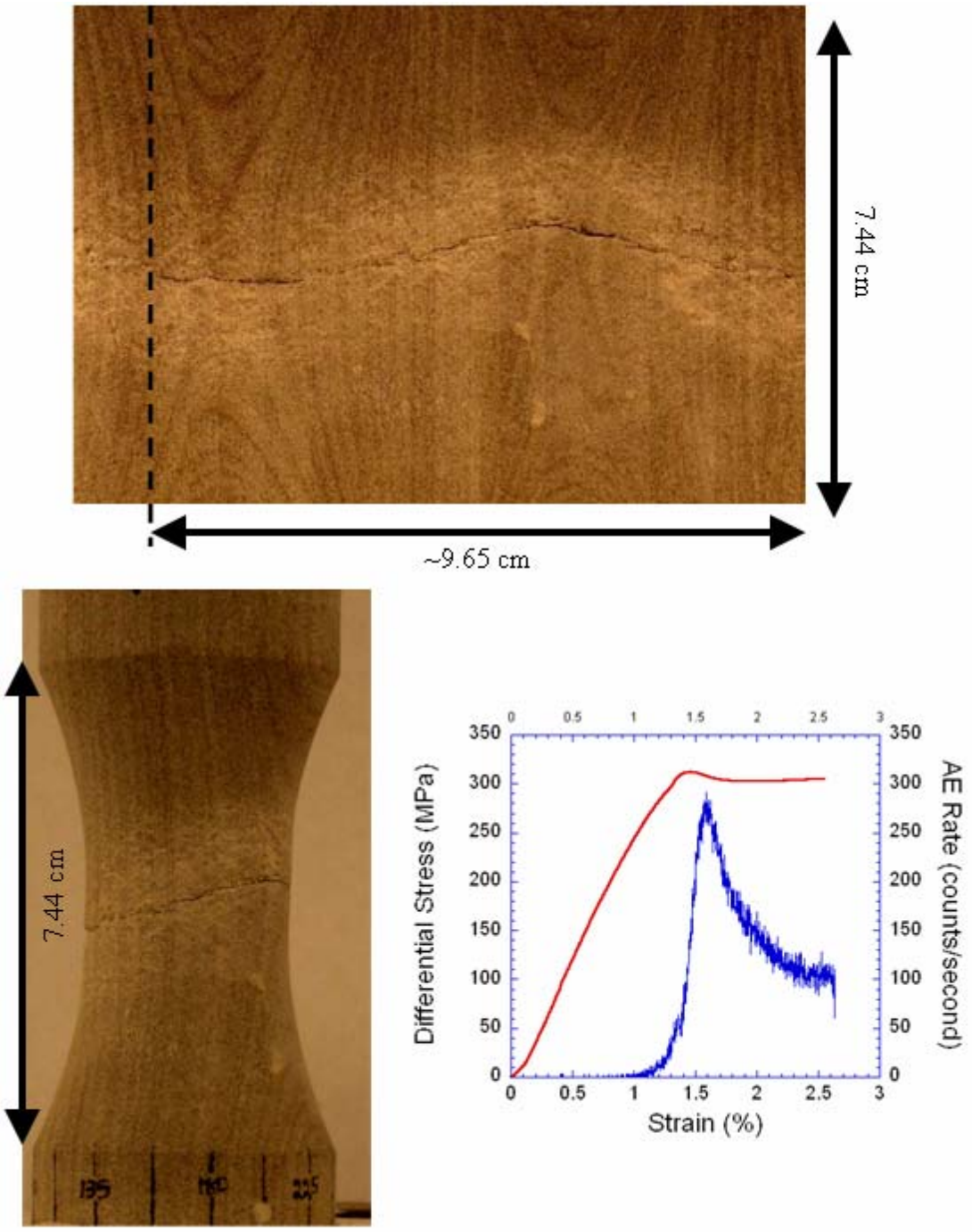

Figure 7. Photograph of a sample deformed at a confining pressure of 100 MPa. The upper photo is a composite photograph of the sample used to determine compaction band angle. The zone of deformation is marked by a sugary texture on the surface of the sample.

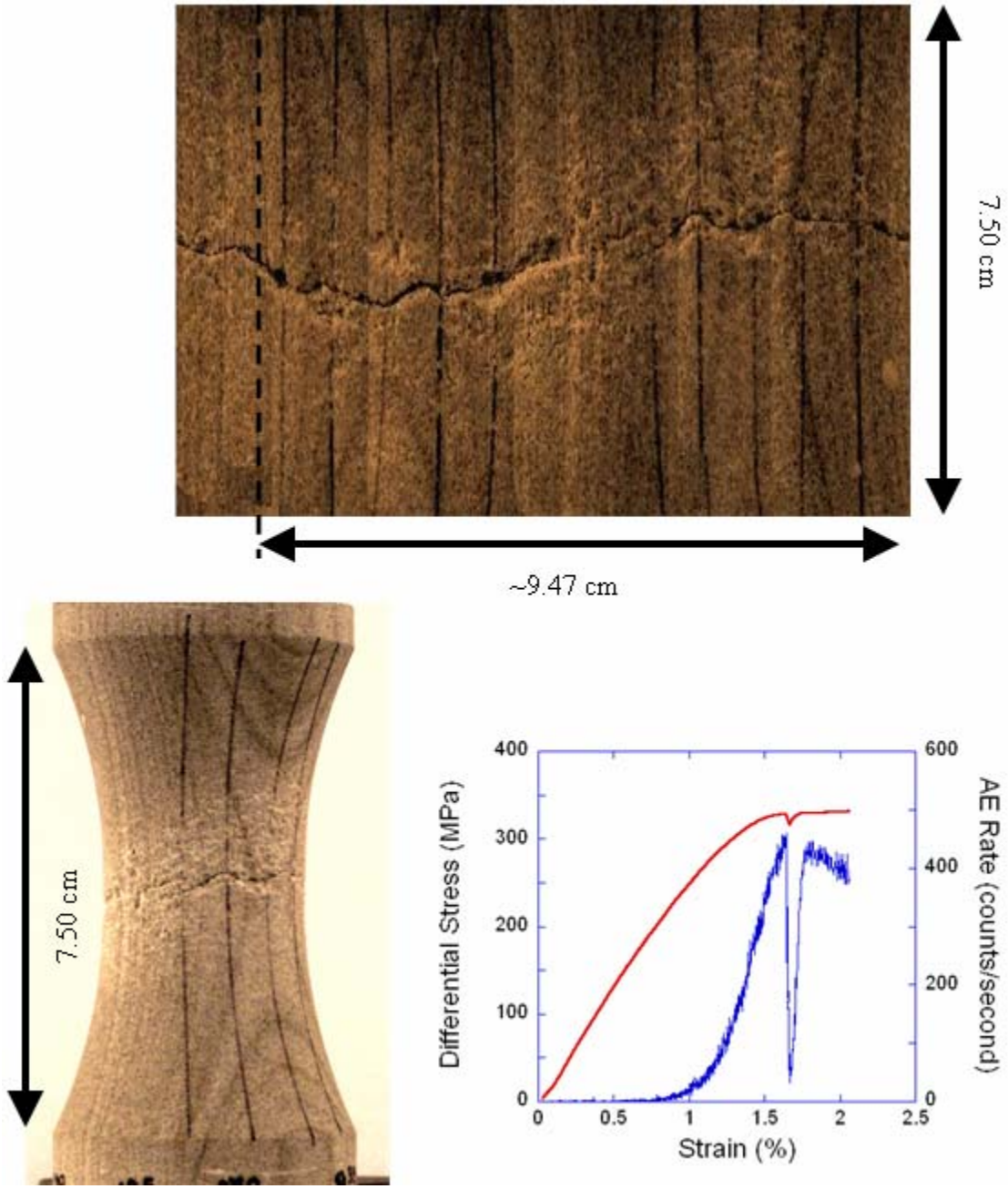

Figure 8. Photograph of a sample deformed at a confining pressure of 150 MPa. The upper photo is a composite photograph of the sample used to determine compaction band angle. The zone of deformation is marked by a sugary texture on the surface of the sample. The drop in differential stress on the stress-strain curve and AE-rate are a result of stopping the LSR during the experiment.

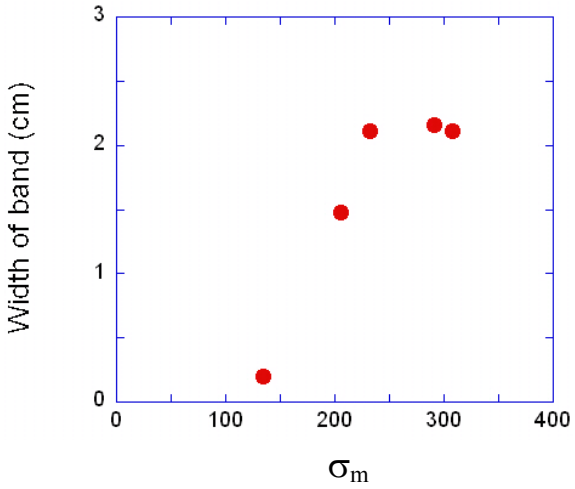

Figure 9. Thickness of deformation bands plotted against mean stress. The width of the band increases with increased confining pressure from 50-200 MPa.

5. DISCUSSION

5.1 Experimental Determination for the Onset of Localization

Acoustic emission activity reflects grain crushing and intergranular slip as a sample is deformed under compression [22]. A marked increase in AE-rate with differential stress is associated with the onset of inelastic strain and the deviation from fairly linear elastic behavior [5], i.e. a gradual yielding of the sample prior to macroscopic failure, as can be seen in Figure 10. During loading prior to macroscopic failure, there is no apparent relationship between rate and confining pressure.

The contrast in the AE-rate after macroscopic failure for different confining pressures may reflect the differences in the relative contribution of microscopic failure mechanisms. AE recorded for samples deformed in the brittle regime is largely due to intergranular cracking and fracturing of the cement [23]. Once macroscopic failure and localization occurs, deformation is concentrated in a thin tabular zone and intergranular cracking is limited to a smaller volume containing smaller (fractured) grains causing the significant decrease in AE-rate. AE recorded for samples deformed in the ductile regime is a result of grain crushing and pore collapse [23]. After macroscopic failure, the deformation is again confined to a tabular zone; however, at high mean stresses the deformation band encompasses a broader zone of material and the band thickness may increase with continual shortening. Accordingly, the AE-rate does not fall off as quickly, or not at all, at the higher confining pressures.

Typically, macroscopic failure is determined to coincide with the rollover of the

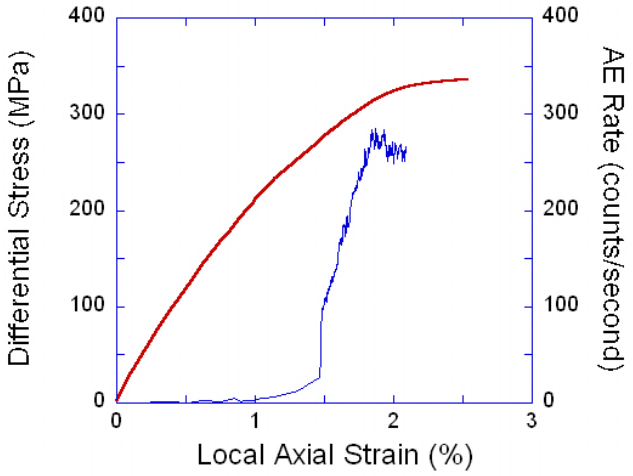

Figure 10. Comparison of differential stress and AE-rate during differential loading for confining pressure of 200 MPa (local axial strain). Changes in slope of the AE rate curve identified by some are thought to reflect the deformation in the sample.

stress-strain curve, but this method is not well defined. A study done by DiGiovanni [12] for triaxial compression of cylindrical samples identified two peaks in the AE-rate curves. The first is associated with deformation in the sample ends and the second due to the propagation of the deformation band. The first peak in AE-rate is not present in the data from this study because end effects are minimized by the dogbone sample geometry. The second peak seen in DiGiovanni's [12] study correlates to the marked change in slope of the AE-rate curve identified in this study and presumably can be used as a more precise determination of the point of macroscopic failure and band formation. This observation is supported by the two experiments run at 50 MPa confining pressure. In both these samples there are two distinct deformation bands and the associated AE-rate curves display two peaks. In addition, stress-strain curves display a primary stress drop followed by a smaller, secondary stress drop. Both the stress drops and peaks in AE-rate correlate, and likely relate to the formation of the two intersecting deformation bands in the sample (Figure 6). For compression tests on sandstone by Wong et al. [5], it was also noted that stress-strain curves were marked by stress drops that correlated to the number of deformation bands present within the sample. In following discussion, we assume the inflection in the AE-rate curve denotes the onset of band formation.

5.2 Macroscopic Failure Envelope

Drucker and Prager [24] generalized the von Mises failure criterion to define a yield function for pressure-dependent behavior of an initially isotropic material as

$$f(\sigma_{ij}) = \sqrt{J_2} - k - \mu' I_1/3 = 0$$

where I_1 is the first stress invariant and J_2 is the second stress invariant defined as

$$I_1 = (\sigma_1 + \sigma_2 + \sigma_3)$$

$$\sqrt{J_2} = 1/6\,[(\sigma_2 - \sigma_3)^2 + (\sigma_3 - \sigma_1)^2 + (\sigma_1 - \sigma_2)^2]$$

[10] (Table 2). The material parameter, k, is the strength of the rock when the mean stress is zero, i.e. $I_1 = 0$. The material parameter μ' is the slope of the yield envelope and shows the sensitivity of the yield stress to mean stress [10]. It is an important parameter in calculating the onset of localization and the character of the deformation bands. For compaction bands to form, μ' must be a low-positive to negative number [1, 8, 10]. The yield values for the present experiments are determined at the inflection on the AE-rate curves and plotted in $\sqrt{J_2}$-σ_m space (Figure 11). In Figure 11, the present results are compared to failure strength data from previous work on the same Berea sandstone in triaxial extension experiments on dogbone samples by Bobich [20] and triaxial compression tests on solid cylinders by Cubuk [25]. A yield envelope is fit to the data assuming linear Coulomb-type behavior (i.e., constant μ') at low mean stress and an elliptical cap at high mean stress. Because the failure strength at very high mean stress and P* is not known for this Berea sandstone, the elliptical yield cap is fit to the data assuming that P* is approximately 580 MPa and the BDT occurs at 0.5P* [6]. For subsequent analysis, the values of μ' are determined by finding the slope of the yield envelope nearest the point of interest (Table 3). By this fit, the values of μ' for the present experiments across the BDT change progressively from low-magnitude positive values to progressively negative values with an increase in mean stress.

Table 2
Stress and strain at macroscopic yield

Exp #	Confining Pressure (MPa)	Differential Stress (MPa) *	$\sqrt{J_2}$	Axial Strain (%) **
4911	51.5	249.9	144.3	1.24
4918	50	251	144.9	1.34
4910	102.3	311.9	180.1	1.46
4906	121.2	332.1	191.7	1.8
4919	145	348.4	201.1	2.04
4908	164	381.6	220.3	2.44
4909	187	418.6	241.7	4.78***
4920	195	337.4	194.8	1.77
4912	239.8	365.1	210.8	2.19

* Macroscopic yield based on marked changes in AE rate curve

** Strain averaged over the length of the sample.

*** AE data not recorded

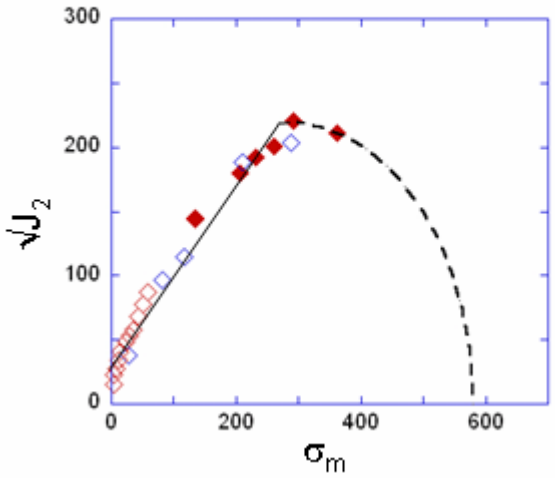

Figure 11. Macroscopic yield envelope fit to triaxial experimental data for Berea sandstone. The solid symbols are yield strengths for this study, open red symbols for triaxial extension tests on dogbone samples [20], and open blue symbols for triaxial compression on solid cylinders [25]. Assumptions for fitting failure envelope are described in the text.

5.3 Predicting the Onset of Localization

According to theory, the hardening behavior of the rock is the key to predicting the onset of localization within a homogeneously deforming specimen [10]. The hardening modulus is defined as

$$h/E = [(\sqrt{3} - \mu')(\sqrt{3} - \beta)]/9\ [h_{tan}/(E-h_{tan})],$$

where E is Young's modulus determined from the slope of the elastic portion of the stress-strain curve, h_{tan} is the slope of the stress-strain curve as it evolves with shortening, and β is the dilatancy factor. The critical hardening modulus for localization is defined as

$$h_{cr}/E = (\mu' - \beta)^2 / [18(1 - \nu)] - (\mu' + \beta + 3N)^2 / 36,$$

where N is the normalized intermediate principal deviatoric stress, which in triaxial compression may be defined as

$$N = -(\sigma_2 - (\sigma_1 + \sigma_2 + \sigma_3)/3) / \sqrt{J_2}.$$

In triaxial compression tests , the dilatancy factor β is defined as

$$\beta = -\sqrt{3}\ R / (3 - R),$$

where

$$R = d\varepsilon^p_{vol} / d\varepsilon^p_{ax},$$

and superscript p indicates inelastic strain components.

According to the original bifurcation analysis, localization occurs when the hardening modulus equals the critical hardening modulus [11]. To test the theoretical predictions for onset of localization in the experiments, the values of h and h_{cr} were calculated directly from the experimental data for the three tests with strain gage

Table 3
Dilatancy factor and slope of failure envelope*

Exp #	Confining Pressure (MPa)	μ'	β
4918	50	0.48	0.218
4919	150	0.133	0.574
4920	200	-1.388	0.592

* determined for the onset of localization.

measurements, and plotted versus differential stress for the complete loading path through failure (Figures 12, 13, and 14). To determine the dilatancy factor, plastic strain components were calculated from the local axial and volumetric strain data by subtracting the linear elastic strains (determined by tangent modulus at low differential stresses) from the total strains. As seen in the plots, the critical hardening modulus decreases from zero to a small-magnitude negative value. From the point where inelastic strain occurs during loading, the hardening modulus progressively evolves from a strong positive value towards zero as the differential stress increases. In the tests, the hardening modulus changes from a positive to negative sign at 251 MPa, 347 MPa, and 335 MPa at low, medium, and high confining pressure, respectively.

At the point where localization is inferred to occur in the experiments, based on the AE-rate data, the hardening modulus is very close to but does not equal the critical hardening modulus, which would suggest the theoretical prediction fails. As shown in the plots (Figures 12, 13, and 14), however, the hardening modulus is rapidly evolving toward the critical value just prior to localization, and it is likely that the strain gages are unable to completely record the local strain just as the deformation band begins to form inside the sample. This explanation is consistent with the fact that a discontinuity in the hardening modulus curve is observed at the inferred point of localization. Prior to the discontinuity, the hardening modulus is rapidly evolving towards the critical value, but just afterwards it changes much more slowly consistent with localization of strain in too small a volume or too distant to be measured by the strain gage. Accordingly, given the level of resolution, the predicted onset of localization in the dogbone experiments agrees

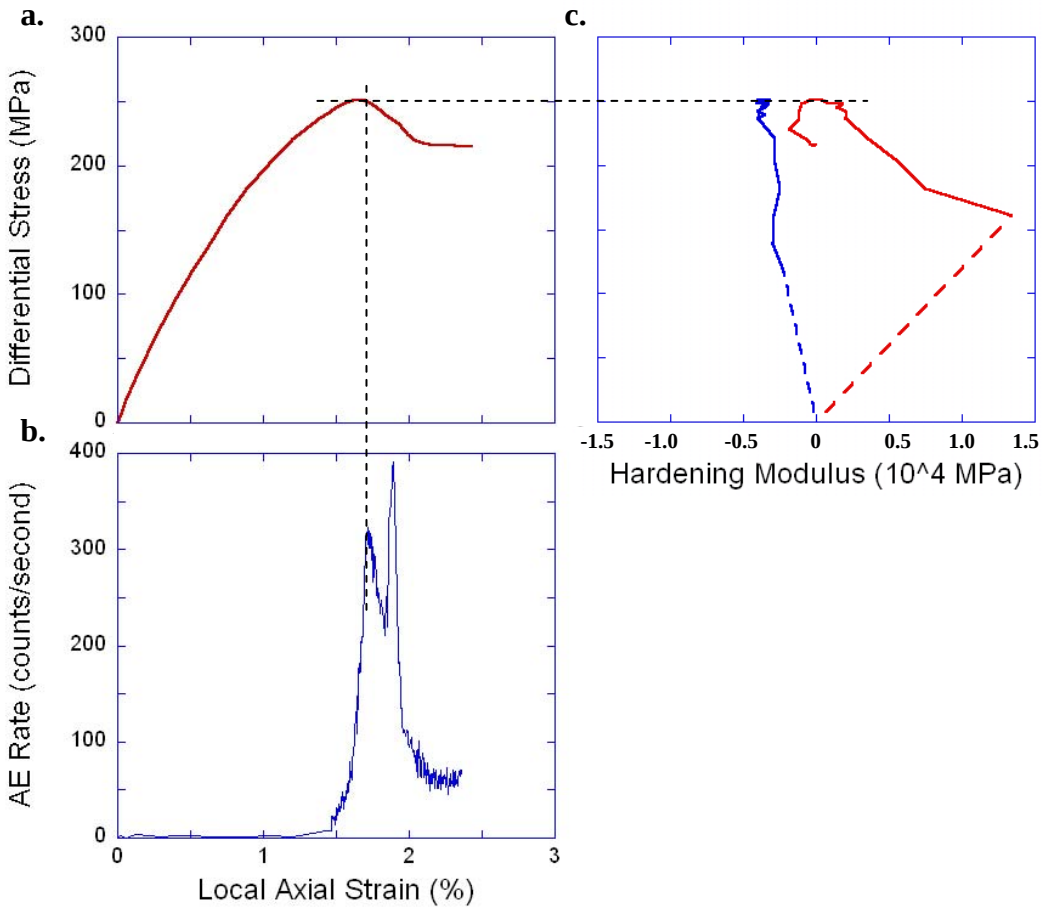

Figure 12. Comparison of AE-rate, differential stress, axial strain rate, and hardening modulus during triaxial compression loading of Berea sandstone at confining pressure of 50 MPa. (a) Differential stress versus axial strain. (b) AE-rate versus axial strain. (c) Hardening modulus (red line) and critical hardening modulus (blue line) versus differential stress. Localization is determined by the abrupt change in AE-rate. The dashed line depicts the correlation between the experimental and predicted onset of localization.

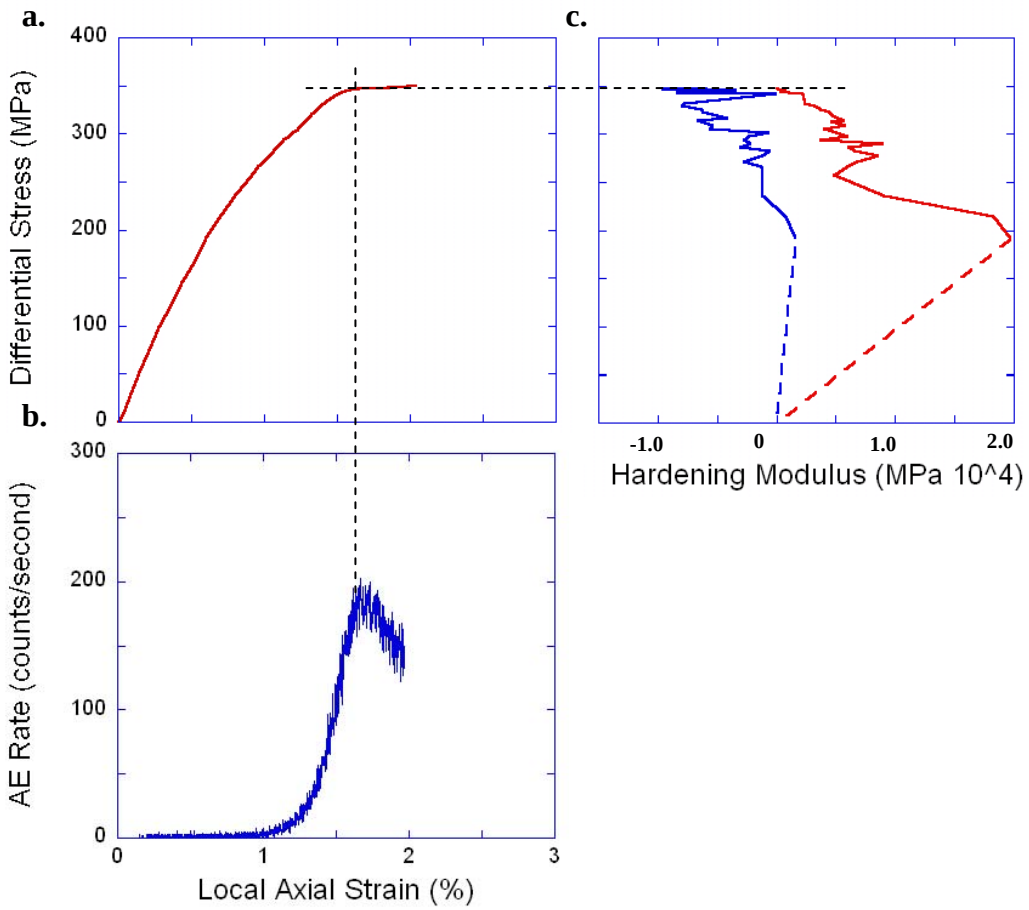

Figure 13. Comparison of AE-rate, differential stress, axial strain rate, and hardening modulus during triaxial compression loading of Berea sandstone at confining pressure of 150 MPa. (a) Differential stress versus axial strain. (b) AE-rate versus axial strain. (c) Hardening modulus (red line) and critical hardening modulus (blue line) versus differential stress. Localization is determined by the abrupt change in AE-rate. The dashed line depicts the correlation between the experimental and predicted onset of localization.

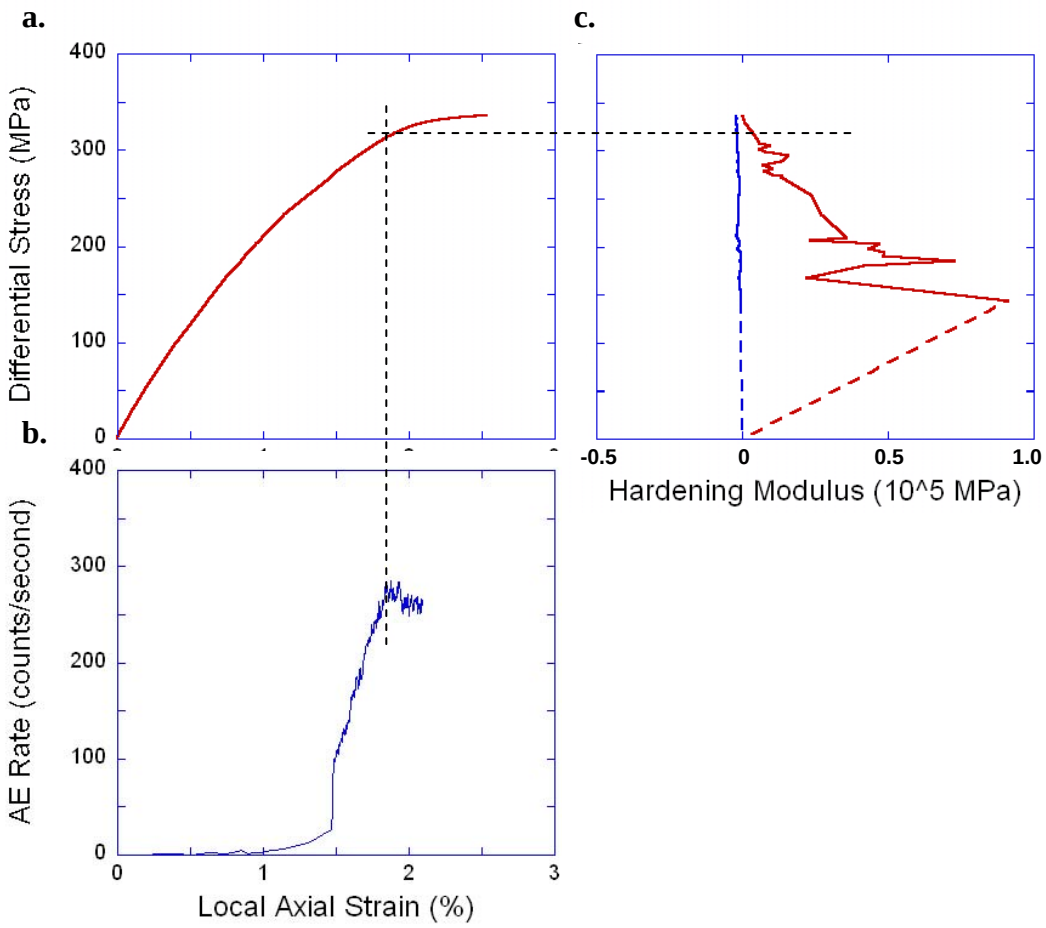

Figure 14. Comparison of AE-rate, differential stress, axial strain rate, and hardening modulus during triaxial compression loading of Berea sandstone at confining pressure of 200 MPa. (a) Differential stress versus axial strain. (b) AE-rate versus axial strain. (c) Hardening modulus (red line) and critical hardening modulus (blue line) versus differential stress. Localization is determined by the abrupt change in AE-rate. The dashed line depicts the correlation between the experimental and predicted onset of localization.

with observation.

For the strain gage tests at confining pressures of 50, 150, and 200 MPa, the dilatancy factor is 0.218, 0.574, and 0.650 at failure, respectively (Table 3). Such small values of dilatancy could indicate that there is a reduction of pore space inside the deformation band [9]. This predicted behavior is not observed at the end of macroscopic failure noted in the volumetric strain curve. The volumetric strain calculated for the sample past macroscopic failure indicates that the deformation is increasingly dilatant with addition shortening. It is possible that if local strains could be measured adequately and β determined for post-localization deformation, the dilatancy factor would have a larger value indicating an increase in pore space.

The predicted values for the dilatancy factor and slope of the yield curve are plotted in β-μ' space (Figure 15), which is a recreation of the failure-mode map from Olsson's [1] paper where the two lines, $\beta + \mu = -\sqrt{3}$ and $\beta + \mu = \sqrt{3}\,(2 - \nu)/(1 + \nu)$, separate the compactant, shear, and dilatant failure fields. The three experiments plot in the shear band zone, the experiments at 50 MPa and 150 MPa in the strain softening region, the other 200 MPa in Figure 15 the strain hardening region. This behavior is reasonable for the sample deformed at 50 MPa, as the onset of localization was determined to occur after macroscopic yield as the sample was deforming by strain softening. The plot is also consistent with the prediction that negative values of h correspond to strain softening [9]. The plot for 150 MPa does not fit with the mechanical behavior of the stress-strain curve. The point plotted for 200 MPa is consistant with the failure curve which shows the sample to continue to deform due to

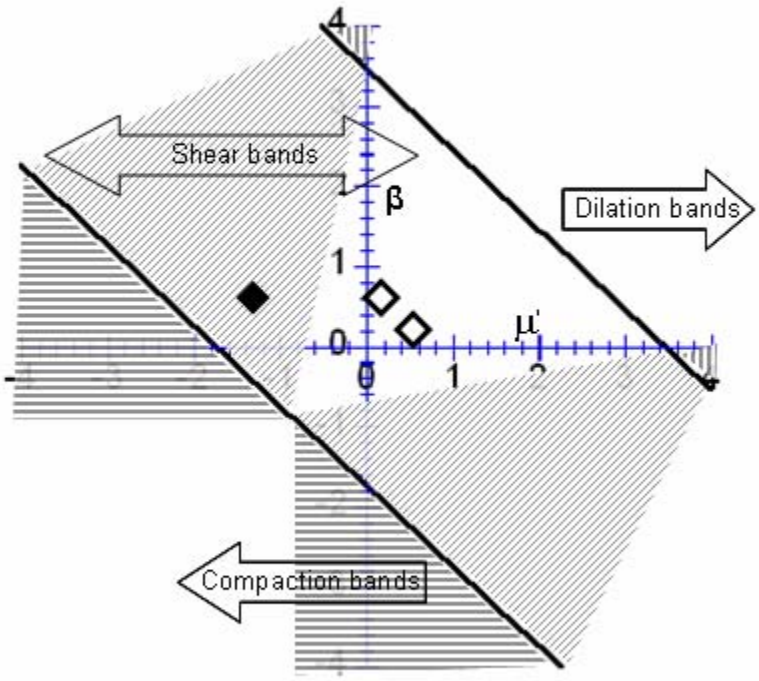

Figure 15. Recreation of the failure mode map for shear bands [1, 10]. The darkened areas represent strain hardening, light areas are strain softening. Data points plotted represent samples deformed at confining pressures of 50 and 150 MPa (open diamond) and 200 MPa (solid diamond).

strain hardening after macroscopic yield.

5.4 Predicting Fracture Orientation

The deformation band angle, measured from the maximum principal stress axis, is expected to increase with increased confining pressure [9]. In field examples, pure compaction bands in the field are interpreted to have propagated perpendicular to the maximum principal stress axis, i.e. a band angle of 90º [2]. Using the dilatancy factor and slope of the yield envelope, the fracture angle, θ, is given by

$$\theta = \pi/4 - \tfrac{1}{2} \arcsin(\alpha),$$

where

$$\alpha = 2\sqrt{3}/9 \, (1 + \nu) \, (\mu' + \beta) - (1 - 2\nu)/3$$

[10]. For experiments with strain gage data, the predicted deformation band angles are 44º for a confining pressure of 50 MPa, 42º for a confining pressure of 150 MPa, and 62º for a confining pressure of 200 MPa. The measured orientation of the deformation bands on the samples deformed at 50, 150, and 200 MPa are 37º, 59º, and 70º, respectively. The model predicts the general trend correctly, but the absolute values differ by 7-17º and the observed values show much greater range in orientation (Table 4).

Previous studies also note discrepancies between predicted and observed deformation band angles [1]. Besuelle [9] reports that the greatest difference between predicted and observed band angles, up to 13º, occurs at low confining pressure. One possible cause for the discrepancy in the present study is that predictions are for the orientation of bands at the onset of localization, whereas observations are made of

samples shortened well beyond macroscopic yield. In this suite of experiments, samples were deformed up to 1% additional axial strain after onset of localization.

Future work should document the nature (geometry, orientation, microstructure) of the deformation bands as a function of shortening. To this end, study of the samples from the strain gage experiments would be particularly valuable as these were not deformed much beyond the inferred point of localization.

Table 4
Comparing the observed band orientation to the predicted band orientation

Exp #	Confining Pressure (MPa)	$\theta_{observed}$	$\theta_{predicted}$
4918	50	37	44
4919	150	59	36
4920	200	70	62

6. CONCLUSION

In order to accurately measure local strains and stress states in a sample as localization occurs, it is necessary to use a sample geometry that limits end effects and other marked stress heterogeneities, but also allows for direct measurement of local strains. For these experiments, the dogbone geometry (typically used for extension and hybrid fracture experiments) was a good choice. Deformation was forced to occur in the neck of the sample away from the ends due to the smaller neck diameter, and band geometry does not appear to be affected by the curvature of the sample neck. Also, having the smooth outer surface with large radius of curvature allows for strain gages to be affixed on the sample surface and for local strains to be measured as the sample is deformed.

The primary purpose of the experiments was to determine if the onset of localization predicted by bifurcation analysis was supported by direct observation of samples deformed in the laboratory across the brittle to ductile transition. For this study, the onset of localization was identified on the basis of a marked change in the AE-rate curve. A peak or marked change in the AE-rate is thought to coincide with the onset of localization of deformation within a sample. The experimental observations are consistent with the onset of localization predicted by bifurcation analysis.

Measurements of the deformation band orientation in samples deformed across the BDT, for 50 MPa to 250 MPa confining pressure, show an increase in band orientation from 35º to 80º (as measured from the maximum principal stress). This is a

much greater change in band orientation with increased confining pressure than is predicted by bifurcation analysis. This discrepancy may relate to the problem that bifurcation analysis is used to predict the onset of localization, while the deformation bands have undergone strains past the onset of localization. In addition, during macroscopic failure the samples are more dilatant than would be predicted by the models. Again, this may be a reflection of measuring the end-product of deformation well past macroscopic failure in experiments whereas model predictions apply to the onset of localization. An independent measurement to better define the character of the band at the point of localization over high and low confining pressures is needed to further test theoretical models.

REFERENCES

[1] Olsson WA. Theoretical and experimental investigation of compaction bands in porous rock. Journal of Geophysical Research 1999; 104: 7219-7228.

[2] Mollema PN, Antonellini MA. Compaction bands: a structural analog for anti-mode I cracks in aeolian sandstone. Tectonophysics 1996; 267: 209-228.

[3] Davatzes NC, Aydin A, Eichhubl P. Overprinting faulting mechanisms during the development of multiple fault sets in sandstone, Chimney Rock fault array, Utah, USA, Tectonophysics 2003; 363: 1-18.

[4] Antonellini MA, Aydin A, Pollard DD., Microstructure of deformation bands in porous sandstones at Arches National Park, Utah. Journal of Structural Geology 1994; 16: 941-959.

[5] Wong T-f, Baud P, Klein E. Localized fault modes in a compacted porous rock. Geophysical Research Letters 2001; 28: 2521-2524.

[6] Wong T-f, David C, and Zhu W. The transition from brittle faulting to cataclastic flow in porous sandstones: mechanical deformation. Journal of Geophysical Research 1997; 102: 3009-3025.

[7] Issen KA, Rudnicki JW. Conditions for compaction bands in porous rock. Journal of Geophysical Research 2000; 105: 21529-21536.

[8] Rudnicki JW. Shear and compaction band formation on an elliptical yield cap. Journal of Geophysical Research 2004; 109: B03402, doi:10.1029/2003JB002633.

[9] Besuelle P. Compacting and dilating shear bands in porous rock: theoretical and experimental conditions. Journal of Geophysical Research 2001; 106: 13,435-13,442.

[10] Paterson MS, Wong T-f. Experimental rock deformation - the brittle field. Berlin: Springer, 2005.

[11] Rudnicki JW, Rice JR. Conditions for the localization of deformation in pressure-sensitive dilatant materials. Journal of the Mechanics and Physics of Solids 1975; 23: 371-394.

[12] DiGiovanni AA. Micromechanics of compaction in an analogue reservoir sandstone. Proceedings of the North American Rock Mechanics Symposium 2001; 4: 1153-1160.

[13] Vajdova V, Wong T-f. Incremental propagation of discrete compaction bands: acoustic emission and microstructural observations on circumferentially notched samples of Bentheim. Geophysical Research Letters 2003; 30.

[14] Aydin A, Johnson AM. Development of faults as zones of deformation bands and as slip surfaces in sandstone. Pure and Applied Geophysics 1978; 116: 931-942.

[15] Davatzes NC, Eichhubl P, Aydin A. Structural evolution of fault zones in sandstone by multiple deformation mechanisms. Moab fault, southeast Utah, Geological Society of America Bulletin 2005; 117: 135-148.

[16] Tondi E, Antonellini M, Aydin A, Marchegiani L, Cello G. The role of deformation bands, styolites and sheared styolites in fault development in carbonate grainstones of Majella Mountain, Italy. Journal of Structural Geology 2006; 28: 376-391.

[17] Bésuelle P, Desrues J, and Raynaud S. Experimental characterisation of the localisation phenomena inside a Vosges sandstone in a triaxial cell. International Journal of Rock Mechanics and Mining Sciences 2000; 37: 1223-1237.

[18] Baud P, Klein E, and Wong T-f. Compaction localization in porous sandstones: spatial evolution of damage and acoustic emission activity. Journal of Structural Geology 2004; 26: 603-624.

[19] Tembe S, Vardoulakis I, Wong T-f, Zhu W. Initiation and propagation of strain localization in circumferentially notched samples of two porous sandstones. Journal of Geophysical Research 2006; 111: B02409, doi:10.1029/2005JB003611.

[20] Bobich JK. Experimental analysis of the extension to shear fracture transition in Berea sandstone. M.S. thesis. Texas A&M University, 2005, 1-60

[21] Ramsey JM, Chester FM. Hybrid fracture and the transition from extension fracture to shear fracture. Nature 2004; 428: 63-66.

[22] Lockner D., The role of acoustic emission in the study of rock fracture. Int J Rock Mechanics & Mining Sciences 1993; 30: 883-900.

[23] Menendez, B., Zhu, W. and Wong, T.-f., Micromechanics of brittle faulting and cataclastic flow in Berea sandstone. Journal of Structural Geology 1996; 18: 1-16.

[24] Drucker DC, Prager W. Soil mechanics and plastic analysis or limit design. Q Appl Math 1952; 10: 157-165.

[25] Cubuk P. Experimental study of fracture development in multilayers of contrasting strength and ductility, M.S. thesis, Texas A&M University 2002, 1-65

VITA

ELIZABETH ANNE HERRIN

Dept. of Geology & Geophysics, MS 3115,
Texas A&M University, College Station, TX 77843
eherrin@tamu.edu

Education

M.S., Geology, Texas A&M University, College Station, TX, December 2008

B.S., Geology, Texas A&M University, College Station, TX, May 2005

Association Memberships

- American Association of Petroleum Geologists
- Geological Society of America

Professional Experience

Texas A&M University Geology & Geophysics Dept. College Station, TX
Teaching Assistant August 2005-May 2008
Taught Mineralogy, Field Methods, and Structural Geology Labs

Dominion Exploration & Production Oklahoma City, OK
Geology Intern May-August 2007
3-D Seismic Interpretation

Dominion Exploration & Production New Orleans, LA
Geology Intern May-August 2006
3-D Seismic Interpretation

Dominion Exploration & Production Houston, TX
Geology Intern May-August 2005
East Texas Regional Analysis